Research Article

Journal of Environmental Nanotechnology

Green-synthesized *Bryophyllum pinnatum*-PVP/Ferric Oxide Nanoparticles: Antibacterial and Cytocompatibility Studies

Krishna Kumari[1], Ajay Ravi[2], C. Naveen[3] and Sorimuthu Revathi[4]*

[1]Department of Undergraduate Medical Education, Saveetha Medical College and Hospital, Saveetha Institute of Medical and Technical Sciences, Chennai, TN, India

[2]Department of Orthopaedics, Saveetha Medical College and Hospital, Saveetha Institute of Medical and Technical Sciences, Chennai, TN, India

[3]Department of Pharmacology, 2D Nanomaterial Material Science Lab, Saveetha Medical College and Hospital, Saveetha Institute of Medical and Technical Science, Thandalam, Chennai, TN, India

[4]Department of Emergency Medicine, Saveetha Medical College and Hospital, Saveetha Institute of Medical and Technical Science, Thandalam, Chennai, TN, India

Received: 16.07.2026 Accepted: 10.08.2026 Published: 30.09.2026

*revathis1598@gmail.com

ABSTRACT

The development of environmentally sustainable nanomaterials has attracted considerable attention for biomedical applications due to their enhanced biocompatibility and reduced environmental impact. In the present study, *Bryophyllum pinnatum*-functionalized polyvinylpyrrolidone (PVP)-stabilized ferric oxide nanoparticles (BP–Fe@PVP) were successfully synthesized using a simple one-pot green synthesis approach using *B. pinnatum* leaf extract as a natural reducing and capping agent. The synthesized NPs were comprehensively characterized using UV–Visible spectroscopy, FTIR, FESEM–EDX, XRD, DLS, and zeta potential analysis. NP formation was confirmed by 419nm UV-Vis peak and crystalline FeO phase by XRD. FTIR and EDX demonstrated that BP bioactive compounds, PVP, and the elemental composition stabilized the NPs. FESEM showed uniform nanoscale morphology, while DLS and zeta potential confirmed good size distribution and colloidal stability. The antibacterial activity of BP–Fe@PVP NPs showed concentration-dependent inhibition against *Escherichia coli*, *Staphylococcus aureus*, *Pseudomonas aeruginosa*, and *Klebsiella pneumoniae,* with the highest activity observed at 100 µg/mL. Cytotoxicity evaluation using HFF-2 human fibroblast cells demonstrated high cell viability across all tested concentrations, indicating excellent cytocompatibility, which was further supported by morphological observations. Overall, the produced BP–Fe@PVP NPs showed acceptable biocompatibility, broad-spectrum antibacterial activity, and suitable physicochemical properties, indicating their promise as an environmentally benign nanomaterial for future pharmaceutical and biomedical applications.

Keywords: *Bryophyllum pinnatum*; Nanotechnology; Polyvinylpyrrolidone; Antibacterial activity; Cytocompatibility; Medicine.

1. INTRODUCTION

Cell viability and proliferation are fundamental indicators of cellular health and play a critical role in evaluating the biological safety and therapeutic potential of newly developed nanomaterials(Elumalai *et al.* 2023). Various physical and chemical agents can adversely affect cell survival by disrupting membrane integrity, inducing oxidative stress, inhibiting protein synthesis, damaging DNA, or interfering with essential enzymatic pathways(Khalef *et al.* 2024; Lakshmikanthan *et al.* 2026). Consequently, in vitro cytotoxicity assays have become indispensable tools for assessing the biocompatibility and biological activity of nanomaterials before their clinical application. Among these, the MTT assay is one of the most widely employed methods owing to its simplicity, reproducibility, cost-effectiveness, and ability to rapidly evaluate cell metabolic activity and viability (Jayakumar *et al.* 2021; Khalef *et al.* 2024). In vitro cytotoxicity assays have gained increasing importance in biomedical research, particularly in cancer therapeutics, where they are routinely used to investigate the anticancer potential of newly synthesized compounds while reducing the dependence on animal experimentation (Lomphithak and Fadeel, 2023).

The distinct physicochemical characteristics of NPs, such as their high surface area, improved surface reactivity, shape, and superior biological activity, have made nanotechnology one of the most promising areas of biomedical science (Kazi *et al.* 2025). These distinctive characteristics have enabled Nps to be explored in many biomedical applications, including targeted drug delivery, bioimaging, tissue engineering, antimicrobial therapy, biosensing, and cancer treatment (Barai, 2026). Among various nanomaterials, FeO Nps have attracted considerable attention owing to their excellent chemical stability, magnetic properties, biocompatibility, and low

toxicity. Their ability to generate ROS under specific biological conditions, coupled with their facile surface functionalization, makes them promising candidates for cancer therapy, targeted drug delivery, MRI, and hyperthermia applications (Dowlath *et al.* 2021).

Recently, environmentally sustainable approaches for Nps synthesis have received increasing attention as alternatives to conventional chemical and physical methods. Biomedical applications are limited by the use of dangerous reducing agents, high temperatures, and toxic byproducts in traditional synthetic processes (Ahmed *et al.* 2026; Kumar *et al.* 2026). In contrast, green synthesis utilizes biological resources such as plants, microorganisms, and natural biomolecules as reducing and stabilizing agents, providing an eco-friendly, economical, and scalable route for NP fabrication(Parthiban *et al.* 2019). Plant-derived phytochemicals can contribute to the green synthesis and stabilization of nanomaterials, providing a sustainable alternative to conventional chemical approaches (Shahzadi *et al.* 2025; Sivaranjani and Parthiban, 2025; Hema *et al.* 2025).

Bryophyllum pinnatum (Lam.) (BP) Oken, a medicinal plant belonging to the Crassulaceae family, has long been recognized for its extensive therapeutic properties in traditional medicine. Native to Madagascar and now widely distributed throughout tropical and subtropical regions, the plant has traditionally been used for the treatment of wounds, inflammation, infections, kidney disorders, hypertension, and various inflammatory conditions(Sharma *et al.* 2024). Phytochemical investigations have demonstrated that *B. pinnatum* (BP) contains numerous bioactive compounds, including flavonoids, bufadienolides, triterpenoids, phenolic compounds, and organic acids, which exhibit antioxidant, anti-inflammatory, antimicrobial, and anticancer activities(Siddiqui *et al.* 2025; Sneha, 2025). These phytoconstituents also serve as effective reducing and capping agents during green NP synthesis, thereby enhancing NP stability and biological performance(Arul *et al.* 2015; Jovita and Naveen, 2026).

To further improve NP stability and dispersibility, polymeric stabilizers are frequently incorporated during synthesis. PVP is one of the most extensively utilized biocompatible polymers because of its excellent water solubility, chemical inertness, low toxicity, and strong steric stabilization capability(Sebastian Espinel *et al.* 2024). PVP effectively prevents NP aggregation by forming a protective coating around the NP surface, thereby improving colloidal stability, increasing surface accessibility, and enhancing biological interactions. Furthermore, PVP has been widely applied in pharmaceutical formulations, controlled drug delivery systems, tissue engineering, wound healing materials, and nanomedicine owing to its excellent biocompatibility and regulatory acceptance (Jaafreh *et al.* 2026).

Several studies have reported the green synthesis of NPs using medicinal plants; investigations on BP synthesis of Nps their cytotoxic potential remain limited. The synergistic combination of phytochemical-functionalized FeO NPs with PVP stabilization is expected to improve NP stability, cellular interactions, and therapeutic efficacy while minimizing aggregation and undesirable biological effects(Jagdish and Nehra, 2022; Sahu *et al.* 2026). Furthermore, the presence of compounds on the NP surface may enhance cellular uptake and contribute to oxidative stress based cytotoxicity against cancer cells while maintaining acceptable biocompatibility(Ayyankalai *et al.* 2025; Ilavenil *et al.* 2025; Jeyanthi *et al.* 2026). Although green synthesis of iron oxide nanoparticles using medicinal plant extracts has been extensively investigated, limited information is available on the development of *Bryophyllum pinnatum*-functionalized PVP-stabilized iron oxide nanoparticles combining plant-derived phytochemicals with polymer-mediated stabilization. In particular, the relationship between *B. pinnatum* phytochemical functionalization, PVP stabilization, physicochemical characteristics, antibacterial performance, and cytocompatibility toward normal human fibroblast cells remains insufficiently explored. Moreover, many previous studies have focused on either plant-mediated iron oxide nanoparticles or polymer-stabilized nanomaterials separately, with limited emphasis on their combined biological performance. Therefore, the present study was designed to develop *B. pinnatum* -functionalized PVP-stabilized iron oxide nanoparticles through a one-pot green synthesis approach and systematically investigate their physicochemical properties, antibacterial activity against clinically relevant pathogens, and cytocompatibility using HFF-2 fibroblast cells.

Therefore, the present study aims to synthesize BP–Fe@PVP through an environmentally friendly green synthesis approach, followed by comprehensive physicochemical characterization and evaluation of their cytotoxic activity using an *in vitro* MTT assay. The aim of this study is expected to provide valuable insights into the development of sustainable plant-mediated FeO NPs with potential applications in cancer therapeutics and other biomedical fields.

2. MATERIALS AND METHODS

2.1 Materials

Dried powder BP were collected from commercial suppliers. Ferric chloride hexahydrate ($FeCl_3 \cdot 6H_2O$, analytical grade), Polyvinylpyrrolidone (PVP, K30 grade), Sodium hydroxide (NaOH) was collected by HiMedia.

2.2 Preparation of *Bryophyllum pinnatum* Leaf Extract

Fresh BP leaves were carefully cleaned using running tap water and double-distilled water. The leaves were cleaned, dried in the shade, and then chopped finely. 10 g of fresh leaf material was cooked for 20 minutes at 60–70°C in 100 mL of double-distilled water. After cooling to room temperature, the extract was filtered using Whatman No. 1 filter paper. Until it was needed, the filtrate was kept at 4°C.

2.3 Green Synthesis of *Bryophyllum pinnatum*-Functionalized PVP-stabilized Ferric Oxide Nanoparticles

An aqueous1mM ferric chloride ($FeCl_3 \cdot 6H_2O$) solution (100 mL) was prepared using double-distilled water. To this solution, 20 mL of BP extract was added dropwise under continuous magnetic stirring. Subsequently, PVP (K30) was added to the reaction mixture at a concentration of 0.5 g, and stirring was continued to achieve uniform dispersion and stabilization of the NPs. The pH of the reaction mixture was adjusted to ~10 using 1 M NaOH solution, and the mixture was stirred continuously for 2 h at room temperature (Adhikari *et al.* 2022; Tyagi *et al.* 2021). The formation of FeO Nps was indicated by the appearance of a reddish-brown precipitate. The reaction mixture was centrifuged at 10,000 rpm for 15 min to collect the Nps. The pellet was washed three times with double-distilled water. The purified NPs were dried at 50–60°C in a hot-air oven, finely powdered, and stored in airtight containers for further physicochemical characterization and cytotoxicity evaluation.

Table 1. Experimental conditions used for the green synthesis of BP−Fe@PVP nanoparticles

Parameter	Experimental Condition
Plant material	*Bryophyllum pinnatum* leaves
Plant extract	10 g leaves / 100 mL distilled water
Extraction temperature	60–70 °C
Extraction time	20 min
Iron precursor	Ferric chloride
Iron precursor concentration	1 mM
Extract volume	20 mL
Iron precursor volume	80 mL
PVP grade	PVP K30
PVP concentration	0.5g
pH	~10
Reaction temperature	Room temperature
Reaction time	2 h
Centrifugation	10,000 rpm
Centrifugation time	15 min
Washing	Distilled water/ethanol
Drying temperature	50–60 °C

2.4 Characterization Strategies

The synthesized BP–Fe@PVP NPs were characterized using complementary analytical techniques to evaluate their optical, functional, morphological, structural, elemental, and colloidal properties. UV–Visible spectroscopy was used to confirm nanoparticle formation and evaluate the optical absorption characteristics of BP–Fe@PVP NPs over the wavelength range of 200–800 nm, with double-distilled water used as the blank. Fourier Transform Infrared (FTIR) spectroscopy was employed to identify the functional groups of *B. pinnatum* phytochemicals and PVP associated with nanoparticle formation, surface functionalization, and stabilization; spectra were recorded using a PerkinElmer Spectrum Two spectrometer in the range of 4000–400 cm^{-1} using the KBr pellet method. Field Emission Scanning Electron Microscopy (FESEM) was used to determine the surface morphology, shape, and approximate particle dimensions of the synthesized nanoparticles, while Energy Dispersive X-ray (EDX) spectroscopy was used to identify their elemental composition and confirm the presence of iron and oxygen along with carbon and other elements associated with the plant-derived and polymeric surface components. X-ray Diffraction (XRD) analysis was performed using a Bruker D8 Advance diffractometer with Cu-Kα radiation ($\lambda = 1.5406$ Å) over a 2θ range of 20–80° to determine the crystalline structure and phase characteristics of the nanoparticles. The crystallite size was estimated using the Debye–Scherrer equation, where D represents crystallite size, λ is the X-ray wavelength, β is the full width at half maximum (FWHM), and θ is the Bragg angle. The obtained diffraction peaks were compared with standard JCPDS reference data for phase identification. Finally, Dynamic Light Scattering (DLS) was used to determine the hydrodynamic particle size and polydispersity index (PDI), providing information on particle-size distribution and dispersion characteristics in suspension, while zeta potential analysis was performed to determine the surface charge and assess the colloidal stability of the nanoparticles. Collectively, these characterization techniques provided comprehensive information regarding the formation, surface functionalization, morphology, elemental composition, crystallinity, particle-size distribution, and colloidal stability of the BP–Fe@PVP NPs.

2.5 Biomedical Applications

2.5.1 Antibacterial Activity

The antibacterial activity of BP–Fe@PVP Nps was evaluated against clinically relevant bacterial pathogens such as *Staphylococcus aureus*, *Escherichia coli*, *Klebsiella pneumoniae*, and *Pseudomonas aeruginosa* using the agar well diffusion method. Fresh bacterial cultures were adjusted to the 0.5 McFarland

turbidity standard and uniformly swabbed onto sterile Mueller–Hinton agar (MHA) plates using sterile cotton swabs. Wells of 6 mm diameter were aseptically punched into the agar using a sterile cork borer. Different concentrations of the BP–Fe@PVP Nps 25, 50, and 100 mg/mL were prepared, and 50 µL of each concentration was added to the respective wells. BP extract was included as the plant control, while amoxicillin was used as the positive control. The inoculated plates were incubated at 37°C for 24 h. Following incubation, the antibacterial activity was assessed by measuring the diameter of the zone of inhibition (ZOI) in millimeters (mm).

2.5.2 In Vitro Cytotoxicity Assay (MTT Assay)

The cytotoxic potential of BP–Fe@PVP Nps was evaluated using the MTT assay on Human Foreskin Fibroblast (HFF-2) cells. HFF-2 cells were cultured in Dulbecco's Modified Eagle Medium (DMEM) supplemented with 10% fetal bovine serum (FBS) and 1% penicillin–streptomycin under standard culture conditions at 37°C in a humidified atmosphere containing 5% CO_2. Cells were seeded into 96-well culture plates and allowed to attach overnight. The cells were then treated with different concentrations of the BP–Fe@PVP Nps (6.25, 12.5, 25, 50, and 100 µg/mL). Untreated cells served as the control. After 24 h of treatment, 20 µL of MTT solution (5 mg/mL) was added to each well and incubated for 4 h. The culture medium was carefully removed, and the resulting purple formazan crystals were dissolved using dimethyl sulfoxide (DMSO). The absorbance was measured at 570 nm using a microplate reader.

Cell viability was calculated using the following equation:

$$\text{cell viability (\%)} = \frac{\text{Absorbance of treated cells}}{\text{Absorbance of control cells}} * 100$$

All experiments were carried out in triplicate, and the results were expressed as mean ± standard deviation (SD).

2.5.3 Morphological Assessment of HFF-2 Cells

Morphological changes in HFF-2 cells following Np treatment were examined using an inverted phase-contrast microscope. Cells treated with 6.25, 12.5, 25, 50, and 100 µg/mL of the BP–Fe@PVP Nps were observed after 24 h of incubation and compared with untreated control cells. Cell morphology was evaluated for changes including cell shape, attachment, spreading, membrane integrity, cytoplasmic shrinkage, cell rounding, and detachment from the culture surface. Representative microscopic images were captured at each concentration to assess concentration-dependent morphological alterations associated with NP exposure.

3. RESULTS

3.1 Green Synthesis of *Bryophyllum pinnatum*-Functionalized PVP-stabilized Ferric Oxide Nanoparticles

A straightforward one-pot approach was used to successfully accomplish the green synthesis of BP–Fe@PVP Nps shows Fig.1. The reaction mixture gradually changed from a light yellow-to-orange solution to a reddish-brown suspension upon the addition of BP extract to the ferric chloride solution containing PVP, signifying the synthesis of FeO NPs(Khan *et al.* 2025). The phytocompounds included in the leaf extract, such as flavonoids, phenolic compounds, terpenoids, and other antioxidant metabolites, are responsible for this apparent color shift by lowering ferric ions while acting as both reducing and capping agents. By using steric stabilization to stop aggregation, PVP substantially improved the stability of the NPs. The elimination of dangerous reducing agents, reduced energy, environmental friendliness, and enhanced biocompatibility are only a few benefits of the one-pot green synthesis approach over traditional chemical procedures. Similar observations have been reported by (Lakshminarayanan *et al.* 2021) synthesized FeO Nps using *Bauhinia tomentosa* leaf extract and observed a distinct colour change during NP formation, attributing the process to the reducing and stabilizing action of plant bioactive compounds. They also demonstrated that phenolic compounds, flavonoids, and terpenoids play a vital role in the nucleation and stabilization of FeO Nps. Overall, the observed colour transformation confirmed the successful green synthesis of BP–Fe@PVP Nps, providing an eco-friendly and sustainable route for preparing biocompatible nanomaterials suitable for subsequent physicochemical characterization and biomedical applications.

3.2 UV–Visible Spectroscopy

The UV–Visible spectra of BP-Fe@PVP are presented in Fig.2. The leaf extract exhibited characteristic absorption bands in the UV region due to the presence of phytoconstituents such as flavonoids and phenolic compounds. After NPs synthesis, the BP-Fe@PVP NPs displayed a distinct absorption peak at 419 nm, confirming the successful formation of FeO NP. The absorption band is attributed to the electronic transition associated with iron oxide nanostructures and indicates the interaction of iron ions with phytochemicals present in the BP extract. The observed absorption peak is in good agreement with previous reports by (Qi *et al.* 2020) Soret absorption band at 419–422 nm for iron-based porphyrin NPs, demonstrating that the slight red shift resulted from coordination between iron and surrounding ligands. Similarly, (Noor *et al.* 2024) reported that *B. pinnatum* leaf extract exhibits characteristic UV absorption bands at 254 and 340 nm, corresponding to its

bioactive phytoconstituents responsible for metal ion reduction and NP stabilization(Sun *et al.* 2011). Therefore, the appearance of the absorption peak at 419 nm confirms the successful green synthesis of BP-Fe@PVP and the effective participation of plant phytochemicals in Np formation.

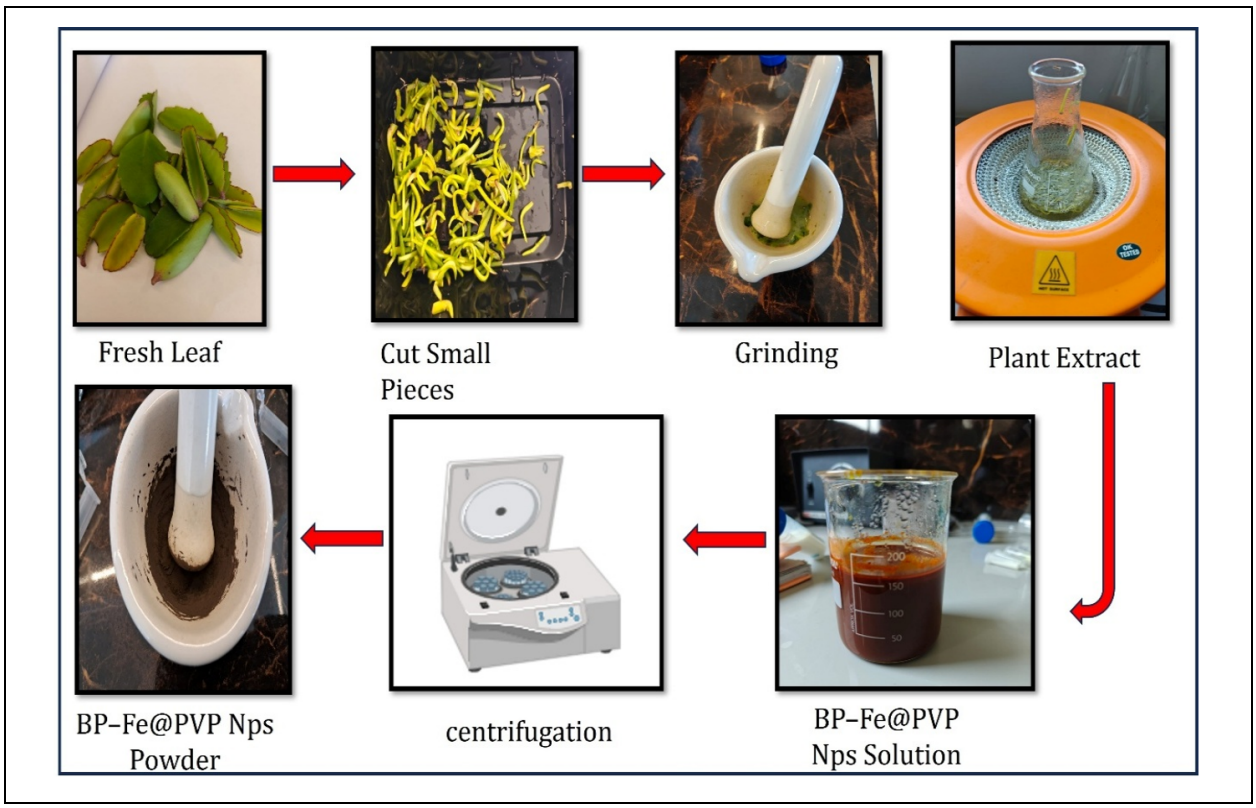

Fig. 1: Schematic representation of the green synthesis of BP-functionalized PVP-stabilized ferric oxide NP

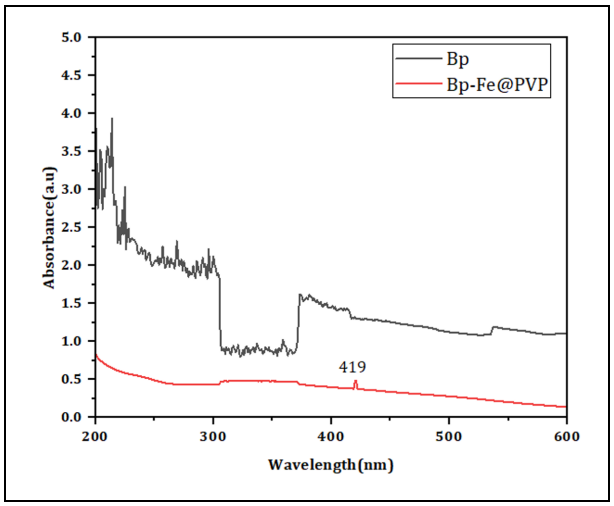

Fig. 2: UV–visible spectra of BP and BP–Fe@PVP

3.3 FESEM and EDX Analysis

The surface morphology of the BP–Fe@PVP was examined using FESEM, and the corresponding micrograph is shown in Fig. 3(A). The NPs exhibited irregularly shaped, granular structures with slight agglomeration. The observed aggregation is attributed to the high surface energy and magnetic interactions of FeO Nps. Nevertheless, the presence of PVP acted as a steric stabilizer, reducing excessive particle agglomeration and improving NP dispersion. Similar observations have been reported by Revathi et al. 2026) and Saravanan et al. 2011), who demonstrated that PVP effectively inhibits NP aggregation by forming a protective layer around the particle surface, thereby enhancing colloidal stability.

The elemental composition of the BP–Fe@PVP NPs was confirmed by EDX analysis Fig.3(B). The EDX

spectrum exhibited characteristic signals corresponding to Fe and O, confirming the successful formation of FeO NPs. The presence of C is attributed to the phytochemical constituents of BP and the PVP polymer coating, whereas minor sodium (Na) and chlorine (Cl) peaks may originate from residual plant metabolites or synthesis precursors(Kiwumulo *et al.* 2022). These findings confirm the successful synthesis of BP–Fe@PVP NPs with the expected elemental composition.

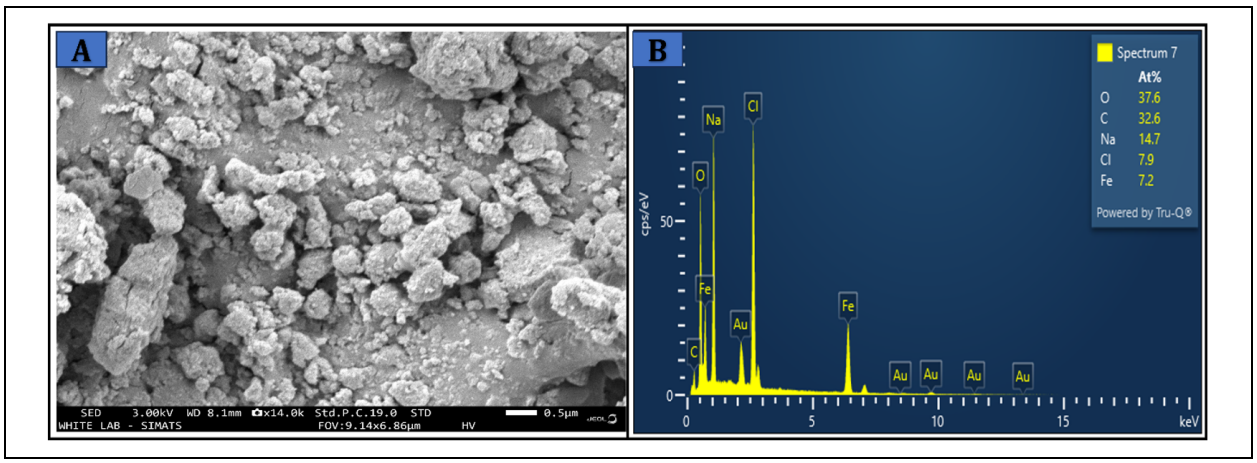

Fig. 3: (A) FESEM micrograph showing the surface morphology of BP–Fe@PVP. (B) EDX spectrum confirming the elemental composition of the synthesized NPs

3.4 Dynamic Light Scattering (DLS) and Zeta Potential Analysis

The hydrodynamic particle size, surface charge, and colloidal stability of the BP–Fe@PVP were evaluated using DLS and zeta potential analysis, as shown in Fig. 4(A–D)(Srivastava *et al.* 2021). The particle size distribution obtained from DLS (Fig.4A) exhibited a single narrow distribution peak, indicating a relatively uniform population of NPs with moderate polydispersity. The hydrodynamic particle size measured by DLS was larger than the particle size observed in FESEM due to the hydration layer surrounding the NPs and the adsorption of PVP molecules in the aqueous medium. Similar observations have been reported for PVP-coated metal NPs, where DLS generally provides larger particle sizes than electron microscopic techniques because it measures the hydrodynamic diameter rather than the actual core size(Lim *et al.* 2013). Recently, (Ielo *et al.* 2025) also reported a narrow particle size distribution for PVP-stabilized silver NPs, demonstrating that PVP effectively limits excessive aggregation and improves colloidal dispersion.

The zeta potential phase (Fig.4B) displayed a single sharp peak, indicating a homogeneous surface charge distribution and good colloidal stability of the synthesized nanocomposite. The negative surface charge can be attributed to the adsorption of plant-derived phytochemicals and PVP molecules on the NP surface, which provide electrostatic and steric stabilization, thereby reducing particle aggregation during storage.

A comparatively consistent particle size distribution and little formation of large aggregates in the NP suspension were confirmed by the autocorrelation function (Fig. 4C), which displayed a smooth decline trend without distinct correlation peaks. The DLS results are supported by this correlation pattern, which is typical of well-dispersed NP systems.

Throughout the analysis, stable electrophoretic conditions were shown by the applied voltage and current profile captured during zeta potential measurement (Fig. 4D). The absence of irregular fluctuations indicates reliable measurement conditions and supports the reproducibility of the obtained zeta potential values. Overall, the DLS and zeta potential analyses demonstrated that the synthesized BP–Fe@PVP nanocomposite possessed a relatively uniform particle size distribution, satisfactory colloidal stability, and effective surface stabilization imparted by both BP phytochemicals and PVP, making the NPs suitable for subsequent biomedical applications.

3.5 X-ray Diffraction (XRD) Analysis

X-ray diffraction was used to examine the crystalline nature and phase purity of the BP–Fe@PVP (Fig.5). The typical crystal planes of crystalline iron oxide NPs are represented by discrete diffraction peaks in the XRD pattern at roughly 30.3°, 35.5°, 43.3°, 53.7°, 57.2°, and 62.8° (2θ). The successful production of a well-crystallized FeO phase was verified by the distinct diffraction peaks. The produced NPs' nanoscale crystallite size is shown by the diffraction peaks' modest broadening.

The average crystallite size was calculated using the Debye–Scherrer equation and was found to be 30.4nm. The presence of PVP did not alter the crystalline structure of the Fe NP but acted primarily as a stabilizing and capping agent during NP synthesis. Similar observations have been reported for PVP-coated NPs, where the polymer improved NP stability without affecting their crystal structure (Saravanan *et al.* 2011). The obtained XRD results therefore confirm the successful BP–Fe@PVP Nps of crystalline suitable for biomedical applications.

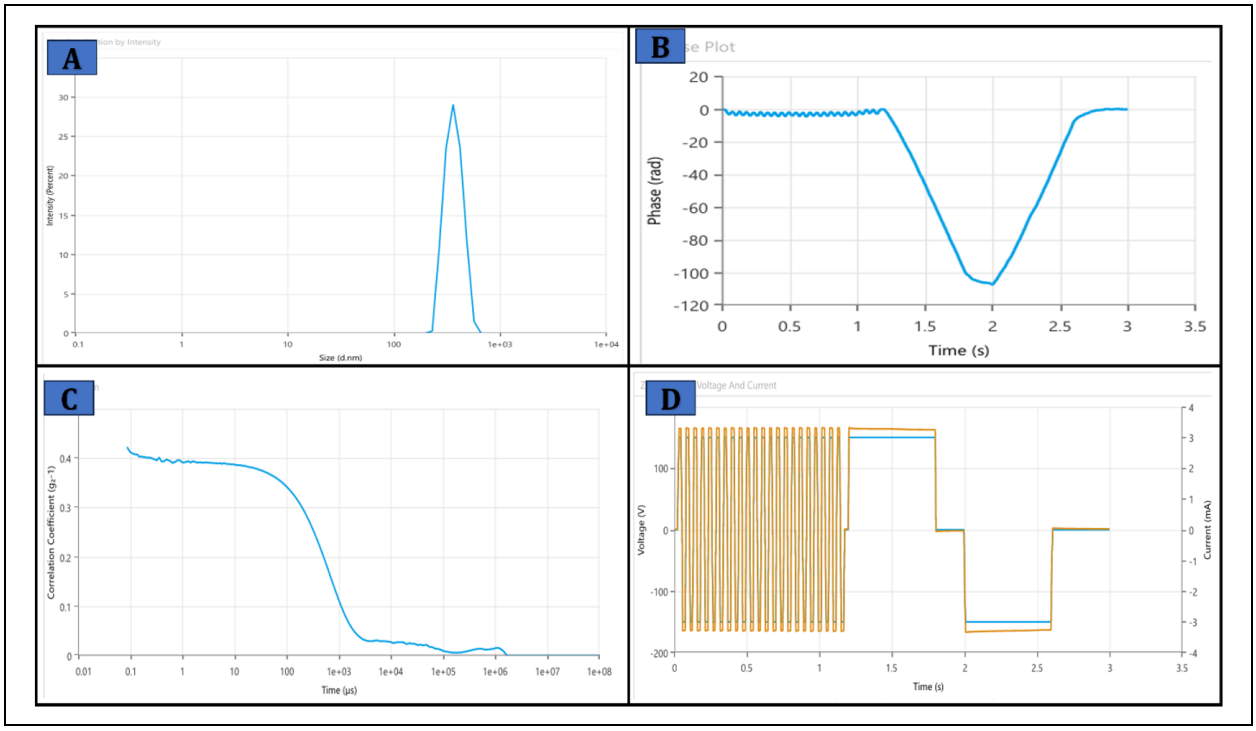

Fig. 4: Shows the particle size distribution, zeta potential phase, autocorrelation function, and voltage/current properties of BP–Fe@PVP as determined by DLS and zeta potential analysis

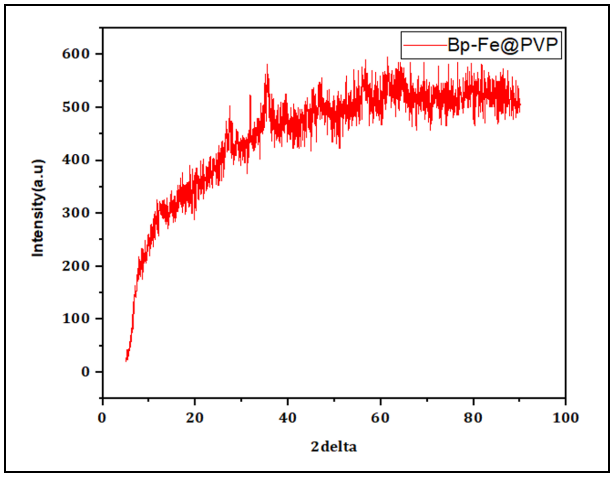

Fig. 5: X-ray diffraction pattern of BP–Fe@PVP for the crystalline iron oxide phase

3.6 Fourier Transform Infrared Spectroscopy (FTIR)

The FTIR spectra of BP–Fe@PVP are presented in Fig.6. The broad absorption band observed at approximately 3319 cm^{-1} corresponds to the O–H stretching vibration of hydroxyl groups present in phenolic compounds and adsorbed water molecules. The peaks at 2234 cm^{-1} and 1628 cm^{-1} are attributed to C–N and C=O stretching vibrations, respectively, indicating the presence of PVP and plant-derived biomolecules on the NP surface. The absorption bands at 1485 cm^{-1} and 1317 cm^{-1} correspond to C–H bending and C–N stretching vibrations of PVP, confirming its successful interaction with the FeO NPs. The peaks observed at 1067 cm^{-1} and 817 cm^{-1} are associated with C–O stretching and aromatic functional groups derived from the phytochemicals of *B. pinnatum*. Furthermore, the characteristic absorption band at 442 cm^{-1} is assigned to the Fe–O stretching vibration, confirming the formation of FeO NPs. The FTIR results demonstrate that the phytochemicals present in BP acted as natural reducing and capping agents, while PVP served as an effective stabilizing polymer by interacting with the NP surface through its carbonyl and nitrogen functional groups. Similar observations have been reported for PVP-coated NPs, where the characteristic C=O and C–N absorption bands confirmed coordination between PVP and metal NPs, leading to enhanced colloidal stability (Bryaskova *et al.* 2011; Saravanan *et al.* 2011). Therefore, the FTIR analysis confirms the successful synthesis and surface functionalization of BP–Fe@PVP nanocomposites.

3.7 Antibacterial Activity

The antibacterial activity of BP–Fe@PVP was evaluated against *Escherichia coli*, *Staphylococcus aureus*, *Pseudomonas aeruginosa*, and *Klebsiella pneumoniae* using the agar well diffusion method of the Fig.7 and Table 2. The synthesized Nps exhibited concentration-dependent antibacterial activity against all tested bacterial strains. Among the three tested concentrations, 100 µg/mL demonstrated the highest antibacterial activity, producing inhibition zones of 20 mm against *E. coli*, 20 mm against *S. aureus*, 20 mm

against *P. aeruginosa*, and 19 mm against *K. pneumoniae*. At 50 µg/mL, the inhibition zones ranged from 15 to 17 mm, while the 25 µg/mL concentration showed comparatively lower antibacterial activity, with inhibition zones between 13 and 17 mm. The BP leaf extract alone exhibited moderate antibacterial activity, producing inhibition zones of 20 mm, 13 mm, 13 mm, and 15 mm against *E. coli*, *S. aureus*, *P. aeruginosa*, and *K. pneumoniae*, respectively. Amoxicillin, the positive control, produced the largest zones of inhibition against all tested bacteria, as was to be expected. The combined actions of FeO NPs, bioactive phytochemicals found in *B. pinnatum*, and the stabilizing action of PVP are responsible for the increased antibacterial activity of BP–Fe@PVP NPs. Because of their enormous surface area, the NPs interact closely with bacterial cell membranes, causing membrane rupture, ROS production, intracellular component leakage, and suppression of vital metabolic activities. Moreover, PVP enhances NP dispersion and promotes increased interaction with bacterial cells, whereas phytochemicals deposited on the NP surface may have synergistic antimicrobial properties. Gram-positive *Staphylococcus aureus* demonstrated susceptibility similar to that of Gram-negative bacteria at the greatest concentration among the tested pathogens. Green-synthesised metal oxide NPs have also been shown to have increased antibacterial activity with increasing NP concentration. Additionally, prior research has shown that due to variations in cell wall permeability and architecture, Gram-positive bacteria are typically more vulnerable to metal oxide NPs than Gram-negative bacteria (Ganvir *et al.* 2026; Noor *et al.* 2024). The results obtained in the present study indicate that BP–Fe@PVP NPs possess broad-spectrum antibacterial activity and may serve as promising antimicrobial nanomaterials for biomedical applications.

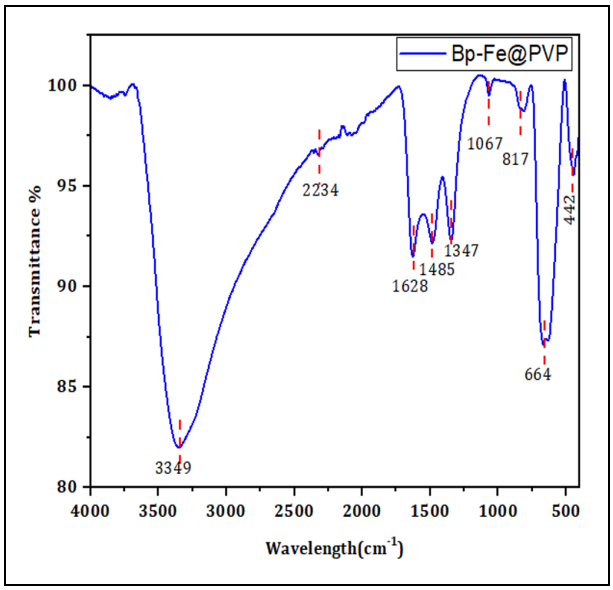

Fig. 6: FTIR spectra of the synthesized BP–Fe@PVP nanocomposite identifying key functional groups

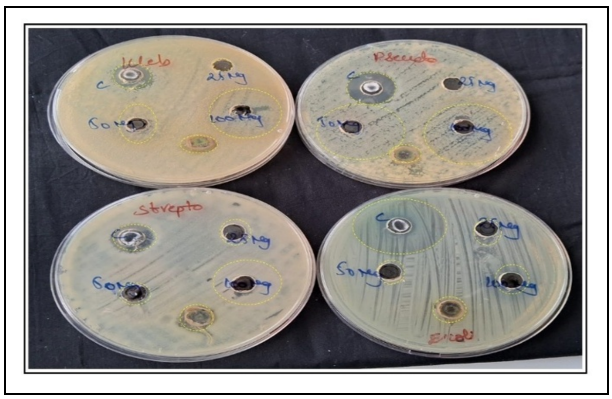

Fig. 7: Antibacterial activity of BP–Fe@PVP nanocomposite against various pathogenic bacteria

Table 2. Zone of inhibition showing the antibacterial activity of *Bryophyllum pinnatum*-functionalized - PVP-stabilized FeO NPs

Microorganism	Control (mm)	Plant Extract (mm)	25 µg/mL (mm)	50 µg/mL (mm)	100 µg/mL (mm)
Escherichia coli	25	20	13	15	20
Staphylococcus aureus	20	13	16	17	20
Pseudomonas aeruginosa	15	13	17	16	20
Klebsiella pneumoniae	20	15	13	15	19

3.8 *In Vitro* Cytotoxicity Assessment

The cytotoxicity of BP–Fe@PVP was evaluated in HFF-2 cells using the MTT assay at concentrations of 6.25, 12.5, 25, 50, and 100 µg/mL. The results are presented in Fig.8. The synthesized NPs exhibited high cell viability across all tested concentrations, indicating good cytocompatibility toward normal fibroblast cells. Although cell viability showed a slight concentration-dependent decrease with increasing NP concentration, more than 80% cell viability was maintained even at the highest concentration (100 µg/mL), suggesting that the synthesized NPs possess minimal cytotoxic effects. The excellent biocompatibility of BP–Fe@PVP NPs may be attributed to the combined effects of BP phytochemicals and the PVP coating, which reduces direct NP cell interactions and improves colloidal stability. The plant-derived bioactive compounds may also contribute to reducing oxidative stress and protecting normal cells from NP-induced damage.

The present findings are in agreement with previous reports demonstrating that green-synthesized NPs exhibit lower toxicity than chemically synthesized NPs because phytochemicals act as natural capping agents. Similarly, studies on BP have reported that its leaf extract possesses a favorable safety profile with no significant adverse effects on renal or hematological parameters following sub-acute administration in

experimental animals, supporting its biocompatibility. Furthermore, green-synthesized metal oxide NPs have been reported to exhibit lower toxicity than conventional NPs owing to their enhanced surface biocompatibility and reduced generation of reactive oxygen species (Noor *et al.* 2024). These findings indicate that BP–Fe@PVP NPs are suitable candidates for further biomedical applications.

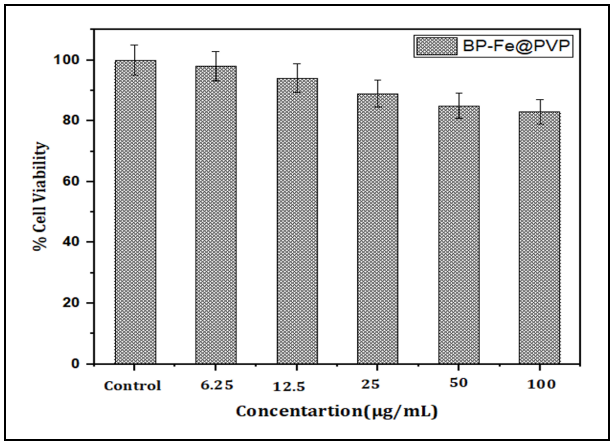

Fig. 8: In vitro cytotoxicity of BP–Fe@PVP in HFF-2 cells (A) cell viability via MTT assay after 24 h treatment with 6.25–100 µg/mL NPs

Data are expressed as mean ± SD (n = 3). Statistical significance was evaluated using one-way ANOVA followed by Tukey's post hoc test, with $p < 0.05$ considered statistically significant.

3.9 Morphological Evaluation of HFF-2 Cells

The morphology of HFF-2 cells following treatment with BP–Fe@PVP NPs was examined using an inverted phase-contrast microscope, and the representative images are shown in Fig. 8B. Untreated control cells exhibited normal fibroblast morphology with elongated spindle-shaped cells, intact cell membranes, and strong adherence to the culture surface. Cells treated with 6.25, 12.5, 25, and 50 µg/mL of BP–Fe@PVP NPs retained normal morphology with minimal observable changes, indicating excellent cellular compatibility. At the highest concentration (100 µg/mL), a slight reduction in cell density and mild cell rounding were observed; the majority of cells remained attached and maintained their structural integrity. No significant membrane damage, extensive cell shrinkage, or widespread cell detachment was detected, corroborating the MTT assay results. The preservation of normal cell morphology further confirms the low cytotoxicity and favorable biocompatibility of the synthesized BP–Fe@PVP NPs toward HFF-2 cells.

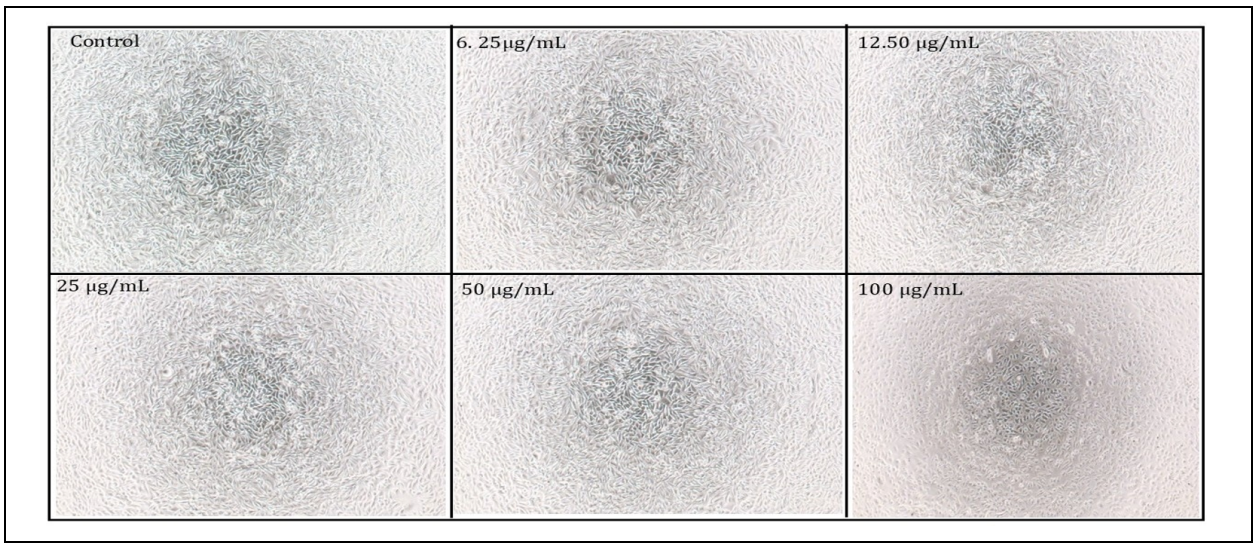

Fig. 9: Morphological evaluation of HFF-2 cells following exposure to BP–Fe@PVP NPs

4. CONCLUSION

In the present study, BP–Fe@PVP NPs were successfully synthesized using a simple, eco-friendly, one-pot green synthesis approach. Bioactive compounds present in *B. pinnatum* effectively acted as reducing and capping agents, while PVP served as a stabilizing polymer to improve nanoparticle dispersion and colloidal stability. The successful formation of the nanocomposite was confirmed by UV–Visible spectroscopy, while FTIR analysis demonstrated the involvement of plant-derived functional groups and PVP in nanoparticle stabilization. FESEM and EDX analyses revealed the formation of nanosized iron oxide nanoparticles with the expected elemental composition. XRD analysis confirmed the crystalline nature of the synthesized nanoparticles, while DLS and zeta potential measurements indicated satisfactory hydrodynamic size distribution and colloidal stability. The BP–Fe@PVP nanocomposite exhibited concentration-dependent antibacterial activity against both Gram-positive and Gram-negative bacterial pathogens, with the highest activity observed at 100

µg/mL. Furthermore, the MTT assay demonstrated good cytocompatibility toward HFF-2 human fibroblast cells, with high cell viability maintained even at the highest tested concentration. Morphological examination further confirmed minimal cellular alterations, supporting the favorable cytocompatibility of the synthesized nanocomposite. Overall, BP–Fe@PVP NPs exhibited desirable physicochemical characteristics, promising antibacterial activity, and favorable biocompatibility. These findings highlight their potential as environmentally friendly multifunctional nanomaterials for future biomedical applications. However, further studies involving detailed mechanistic investigations, in vivo safety evaluation, and therapeutic efficacy are required to establish their biomedical potential.

AUTHOR CONTRIBUTIONS

Krishana Kumari and Naveen: Conceptualization, Methodology, Investigation, Writing – original draft. Ajay Ravi and Naveen: Validation, Formal analysis, Data curation, Software. S. Revathi: Supervision, Project administration, Resources, Funding acquisition, Writing – review & editing. All authors have read and agreed to the published version of the manuscript.

AVAILABILITY OF DATA AND MATERIALS:

All data generated or analyzed during this study are included in this published article.

ACKNOWLEDGMENT

The authors thank the management of SIMATS, Chennai, for providing the necessary infrastructure and support to carry out this research work.

FUNDING

This research received no specific grant from any funding agency in the public, commercial, or not-for-profit sectors.

CONFLICTS OF INTEREST

The authors declare that there is no conflict of interest.

COPYRIGHT

This article is an open-access article distributed under the terms and conditions of the Creative Commons Attribution (CC BY) license (http://creativecommons.org/licenses/by/4.0/).

REFERENCES

Adhikari, A., Chhetri, K., Acharya, D., Pant, B. and Adhikari, A., Green synthesis of iron oxide nanoparticles using Psidium guajava L. leaves extract for degradation of organic dyes and anti-microbial applications, *Catal.*, 12(10), 1188 (2022). https://doi.org/10.3390/catal12101188

Ahmed, R., Manik, K. H., Islam, M. S., Rhine, A., Mim, J. J. and Hossain, N., Green synthesis methods for nanoparticles: Principles, biological routes, and physicochemical approaches toward sustainable nanotechnology, *Next Mater.*, 11, 101929 (2026). https://doi.org/10.1016/j.nxmate.2026.101929

Arul, K. T., Kolanthai, E., Manikandan, E., Bhalerao, G. M., Chandra, V. S., Ramya, J. R., Mudali, U. K., Nair, K. G. M. and Kalkura, S. N., Green synthesis of magnesium ion incorporated nanocrystalline hydroxyapatite and their mechanical, dielectric and photoluminescence properties, *Mater. Res. Bull.*, 67, 55–62 (2015). https://doi.org/10.1016/j.materresbull.2015.02.054

Ayyankalai, N. K., Sundararaj, P., Baskar, M. G., Duraisamy, N., Muthu, S., Lakshmikanthan, M. and Abdi, G., Green production of silver nanoparticles from Cassia occidentalis and Alternanthera pungens and evaluation of their nematicidal activity against Meloidogyne javanica, *Sci. Rep.*, 15(1), 26228 (2025). https://doi.org/10.1038/s41598-025-12096-2

Barai, M., Nanoparticles synthesis, properties and promising devices for drug delivery systems: a review, *Discover Nano.*, 21(1), 208 (2026). https://doi.org/10.1186/s11671-026-04651-1

Bryaskova, R., Pencheva, D., Nikolov, S. and Kantardjiev, T., Synthesis and comparative study on the antimicrobial activity of hybrid materials based on silver nanoparticles (AgNps) stabilized by polyvinylpyrrolidone (PVP), *J. Chem. Bio.*, 4(4), 185–191 (2011). https://doi.org/10.1007/s12154-011-0063-9

Dowlath, M. J. H., Musthafa, S. A., Mohamed Khalith, S. B., Varjani, S., Karuppannan, S. K., Ramanujam, G. M., Arunachalam, A. M., Arunachalam, K. D., Chandrasekaran, M., Chang, S. W., Chung, W. J. and Ravindran, B., Comparison of characteristics and biocompatibility of green synthesized iron oxide nanoparticles with chemical synthesized nanoparticles, *Environ. Res.*, 201, 111585 (2021). https://doi.org/10.1016/j.envres.2021.111585

Elumalai, M., Nagaraj, G., Kasthuri, J., Vellaichamy, E. and Rajendiran, N., Evaluation of cytotoxic activity against A549 human lung cancer cells using green synthesized N-Cholyl D-Penicillamine encapsulated silver and gold nanoparticles, *Inorg. Chem. Commun.*, 153, 110834 (2023). https://doi.org/10.1016/j.inoche.2023.110834

Ganvir, V. Y., Satishkumar, P., Bhaurao Awachat, D., Rani, A., Talodhikar, V. and Krishnaraj, C., Biofabricated CuO Nanoparticle Reinforced Bamboo Fiber Coatings for Photocatalytic Antimicrobial and Superhydrophobic Biomedical Textile Applications, *J. Environ. Nanotechnol.*, 15(2), 330–343 (2026). https://doi.org/10.13074/jent.2026.06.2622243

Ielo, I., Bauso, L. V., Laezza, A., Campione, P., Fabiano, L., Pastorello, M., Marino, A., Laurita, A., Pepe, A., Bochicchio, B., De Luca, G., Messina, G. M. L. and Calabrese, G., In vitro assessment of electrospun PVP+AgNPs scaffolds for bioactive medical use, *Int. J. Mol. Sci.*, 26(18), 9114 (2025). https://doi.org/10.3390/ijms26189114

Ilavenil, K. K., Senthilkumar, V. and Kasthuri, A., Green synthesis of metal nanoparticles from three medicinal plants: a review of environmental and health applications, *Discover Catal.*, 2(1), 3(2025). https://doi.org/10.1007/s44344-025-00007-6

Jaafreh, M., Alshaer, W., Alkawareek, M., Zahari, Z., Alsotari, S., Alqudah, D. A., Choukaife, H., Abbas, M. A., Bustanji, Y. and Alfatama, M., Synergistic antimicrobial nanocomposite: Protamine-loaded PVP-capped silver nanoparticles for combating multidrug-resistant infections, *Asian J. Pharm. Sci.*, 21(3), 101160 (2026). https://doi.org/10.1016/j.ajps.2026.101160

Jagdish, R. and Nehra, K., *Bryophyllum pinnatum* mediated synthesis of zinc oxide nanoparticles: characterization and application as biocontrol agents for multi-drug-resistant uropathogens, *Heliyon*, 8(10), e11080 (2022). https://doi.org/10.1016/j.heliyon.2022.e11080

Jayakumar, M., Ramachandran, M., Krishnaveni, T. and Nattudurai, G., Toxicity and biochemical effects of essential oils of Anethum graveolens L. and Melaleuca cajuputi Powell against Rhyzopertha dominica (F.) (Coleoptera: Bostrichidae), *Int. J. Trop. Insect Sci.*, 41(2), 945–951 (2021). https://doi.org/10.1007/s42690-020-00359-6

Jeyanthi, C. E., Siddheswaran, R., Vijayalakshmi, R. and Ramya, J. R., Multiferroic characteristics of combustion-derived $BiFeO_3$–$Bi_2Fe_4O_9$–CoO nanocomposites, *Mater. Lett.*, 419, 140945 (2026). https://doi.org/10.1016/j.matlet.2026.140945

Jovita, S. and Naveen, C., Bioactive ZnS-reinforced Gellan Gum film enriched with Cucumis maderaspatanus L. blend membrane for antimicrobial application, *South Afr. J. Bot.*, 195, 58–65 (2026). https://doi.org/10.1016/j.sajb.2026.05.003

Hema, K., Anishia, S. R., Rajeswari. S, Padmavathy, V., Sujatha, S. and Thiyagu, M., Green Synthesis and Multifunctional Applications of Moringa Oleifera-enhanced TiO_2 Nanocomposites, *J. Environ. Nanotechnol.,* 14 (1) 7-17 (2025). https://doi.org/10.13074/jent.2025.03.2511225

Kazi, R. N. A., Hasani, I. W., Khafaga, D. S. R., Kabba, S., Farhan, M., Aatif, M., Muteeb, G. and Fahim, Y. A., Nanomedicine: The effective role of nanomaterials in healthcare from diagnosis to therapy, *Pharma.*, 17(8), 987 (2025). https://doi.org/10.3390/pharmaceutics17080987

Khalef, L., Lydia, R., Filicia, K. and Moussa, B., Cell viability and cytotoxicity assays: Biochemical elements and cellular compartments, *Cell Biochem. Funct.,* 42(3), e4007 (2024). https://doi.org/10.1002/cbf.4007

Khan, M. A., Ahmed, M., Abu-Hussien, S. H., Zahid, M. U. and Alharbi, B. F., Green synthesis of iron oxide nanoparticles (Fe_2O_3-NPs) from Citrus Limetta agrowaste for biological and photocatalytic applications, *Sci. Rep.,* 15(1), 33107 (2025). https://doi.org/10.1038/s41598-025-17750-3

Kiwumulo, H. F., Muwonge, H., Ibingira, C., Lubwama, M., Kirabira, J. B. and Ssekitoleko, R. T., Green synthesis and characterization of iron-oxide nanoparticles using Moringa oleifera: a potential protocol for use in low and middle income countries, *BMC Res. Notes.*, 15(1), 149 (2022). https://doi.org/10.1186/s13104-022-06039-7

Kumar, V., Kumar, R., Upreti, M., Puri, K. and Satishkumar, P., Development of a green-synthesized GNP/CQD-reinforced TSP–GG hydrogel bead system for pH-sensitive and sustained doxorubicin release in colorectal cancer therapy, *J. Environ. Nanotechnol.,* 15(2), 31–42 (2026). https://doi.org/10.13074/jent.2026.06.2612081

Lakshmikanthan, M., Abdulla, M., Krishnan, K., Moovendhan, M. and Muthu, S., Anthocyanin-loaded chitosan-alginate nanoparticles from red dragon fruit pulp for targeted therapy against HCT116 colon cancer cells, *Int. J. Biol. Macromol.,* 358, 151739 (2026). https://doi.org/10.1016/j.ijbiomac.2026.151739

Lakshminarayanan, S., Shereen, M. F., Niraimathi, K. L., Brindha, P. and Arumugam, A., One-pot green synthesis of iron oxide nanoparticles from *Bauhinia tomentosa*: Characterization and application towards synthesis of 1, 3 diolein, *Sci. Rep.,* 11(1), 8643 (2021). https://doi.org/10.1038/s41598-021-87960-y

Lim, J., Yeap, S. P., Che, H. X. and Low, S. C., Characterization of magnetic nanoparticle by dynamic light scattering, *Nanoscale Res. Lett.,* 8(1), 381 (2013). https://doi.org/10.1186/1556-276X-8-381

Lomphithak, T. and Fadeel, B., Die hard: cell death mechanisms and their implications in nanotoxicology, *Toxicol. Sci.,* 192(2), 141–154 (2023). https://doi.org/10.1093/toxsci/kfad008

Noor, H., Ayub, A., Dilshad, E., Afsar, T., Razak, S., Husain, F. M. and Trembley, J. H., Assessment of *Bryophyllum pinnatum* mediated Ag and ZnO nanoparticles as efficient antimicrobial and cytotoxic agent, *Sci. Rep.,* 14(1), 22200 (2024). https://doi.org/10.1038/s41598-024-73092-6

Parthiban, E., Ramachandran, M., Jayakumar, M. and Ramanibai, R., Biocompatible green synthesized silver nanoparticles impact on insecticides resistant developing enzymes of dengue transmitted mosquito vector, *SN Appl. Sci.,* 1(10), 1282 (2019). https://doi.org/10.1007/s42452-019-1311-9

Qi, Z. L., Cheng, Y. H., Xu, Z. and Chen, M. L., Recent advances in porphyrin-based materials for metal ions detection, *Int. J. Mol. Sci.,* 21(16), 5839 (2020). https://doi.org/10.3390/ijms21165839

Revathi, S., Dey, N., Thangaleela, S., Kumar, K., Roy, A., Gnanasekaran, L., Shanmugapriya, D., Ali, S., Thomas, A. G. and Sundaram, T., Evaluation of Eupatorium perfoliatum loaded chitosan nanocarriers in silico, in vitro and in vivo for anti-inflammatory, antipyretic and analgesic potential, *Food Biosci.,* 81, 108986 (2026). https://doi.org/10.1016/j.fbio.2026.108986

Sahu, P., Yadav, M. and Shukla, A., Green Synthesis of Silver Nanoparticles using *Bryophyllum pinnatum* (Lam.) and monitoring their antibacterial activities, *J. Drug Deliv. Ther.,* 16(2), 192–197 (2026). https://doi.org/10.22270/jddt.v16i2.7553

Saravanan, L., Diwakar, S., Mohankumar, R., Pandurangan, A. and Jayavel, R., Synthesis, structural and optical properties of PVP encapsulated CdS nanoparticles, *Nanomater. Nanotechnol.,* 1, 17 (2011). https://doi.org/10.5772/50959

Sebastian Espinel, P., Otuna-Hernández, D. S., Davies, R., Spencer, L. and Rodríguez, H., Chitosan and PVP: Versatile biopolymers for drug delivery and advanced materials, *BioNatura.,* 1(3), 23 (2024). https://doi.org/10.70099/bj/2024.01.03.2

Shahzadi, S., Fatima, S., Ul Ain, Q., Shafiq, Z. and Janjua, M. R. S. A., A review on green synthesis of silver nanoparticles (SNPs) using plant extracts: a multifaceted approach in photocatalysis, environmental remediation, and biomedicine, *RSC Adv.,* 15(5), 3858–3903 (2025). https://doi.org/10.1039/d4ra07519f

Sharma, G., Jangra, A., Sihag, S., Chaturvedi, S., Yadav, S. and Chhokar, V., *Bryophyllum pinnatum* (Lam.) Oken: unravelling therapeutic potential and navigating toxicity, *Physiol. Mol. Biol. Plants.,* 30(9), 1413–1427 (2024). https://doi.org/10.1007/s12298-024-01509-7

Siddiqui, T., Kharwar, B., Singh, P. and Kushwaha, A. K., Medicinal potential of *Bryophyllum pinnatum* (Lam.): A detailed review, *Int. J. Res. Ayurveda Pharm.,* 16(6), 153–160 (2025). https://doi.org/10.7897/2277-4343.166231

Sneha, G. and Rashmi, B., *Bryophyllum pinnatum*: A comprehensive review of its phytochemistry and pharmacological activities, *Int. J. Pharma. Sci.,* 3(12), 2987-2994 (2025). https://doi.org/10.5281/ZENODO.17989124

Srivastava, M., Tomer, P., Srivastava, A. and Sharma, S., Fabrication of zero-valent iron nanoparticles by green and chemical reduction methods: Application in the field of antibacterial activities for medicinal point of view, *Int. J. Pharm. Chem. Anal.,* 8(3), 118–122 (2021). https://doi.org/10.18231/j.ijpca.2021.023

Sivaranjani, V. and Parthiban, P., Antioxidant, Antimicrobial, and Potential Biomedical Applications of Green Synthesized Silver Nanoparticles Using Aloe barbadensis Root, *J. Environ. Nanotechnol.*, 14(1), 97-103 (2025) https://doi.org/10.13074/jent.2025.03.2511226

Sun, Z. C., She, Y. B., Zhou, Y., Song, X. F. and Li, K., Synthesis, characterization and spectral properties of substituted tetraphenylporphyrin iron chloride complexes, *Mol.,* 16(4), 2960–2970 (2011). https://doi.org/10.3390/molecules16042960

Tyagi, P. K., Gupta, S., Tyagi, S., Kumar, M., Pandiselvam, R., Daştan, S. D., Sharifi-Rad, J., Gola, D. and Arya, A., Green synthesis of iron nanoparticles from spinach leaf and banana peel aqueous extracts and evaluation of antibacterial potential, *J. Nanomater.,* 2021(1), 4871453 (2021). https://doi.org/10.1155/2021/4871453